Serrat, C., Roca, D., Seres, J. (2015) Coherent amplification of attosecond light pulses in the water-window spectral region. *Optics express*. Vol. 23, Issue 4, pp. 4867-4872. Doi: http://dx.doi.org/10.1364/OE.23.004867.

Serrat, C., Roca, D., Seres, J. (2015) Coherent amplification of attosecond light pulses in the water-window spectral region. *Optics express*. Vol. 23, Issue 4, pp. 4867-4872. Doi: http://dx.doi.org/10.1364/OE.23.004867.

Coherent amplification of attosecond light pulses in the water-window spectral region

C. Serrat,[1,*] **D. Roca,**[1] **and J. Seres**[2]

[1] *Universitat Politècnica de Catalunya, Colom 11, 08222 Terrassa (Barcelona), Spain*
[2] *Institute of Atomic and Subatomic Physics, Vienna University of Technology, Stadionalle 2, 1020 Vienna, Austria*

[*] *carles.serrat-jurado@upc.edu*

Abstract: We present a theoretical study on coherent extreme ultraviolet (XUV) attosecond pulse amplification mediated by nonlinear parametric enhanced forward scattering occurring in the interaction of a strong femtosecond infrared (IR) laser pulse combined with a weak attosecond XUV pulse train with an atom. We predict large amplification of XUV radiation when the IR strong pulse and the XUV weak pulse are optimally phased. We study high-order harmonic processes (HHG) in He, He^{+} and Ne^{++}, and show how although the HHG yield is largely affected by the particular atom used as target, nonlinear parametric XUV amplification is only weakly affected. We conclude that XUV nonlinear parametric attosecond pulse amplification can be most efficiently observed by using atoms with a high ionization potential and that the nonlinear amplification is robust at high photon energies where HHG is not efficient, such as in the *water-window* spectral region.

OCIS codes: (320.0320) Ultrafast optics; (140.7240) UV, EUV, and X-ray lasers.

References and links

1. C. Serrat, "Broadband spectral amplitude control in high-order harmonic generation," Appl. Sci. **2**, 816-830 (2012).
2. C. Serrat, "Broadband spectral-phase control in high-order harmonic generation," Phys. Rev. A **87**, 013825 (2013).
3. C. Serrat, "Coherent extreme ultraviolet light amplification by strong-field-enhanced forward scattering," Phys. Rev. Lett. **111**, 133902 (2013).
4. M. Lewenstein, P. Balcou, M. Y. Ivanov, A. L'Huillier, and P. B. Corkum, "Theory of high-harmonic generation by low-frequency laser fields," Phys. Rev. A **49**, 2117-2132 (1994).
5. J. Seres, E. Seres, D. Hochhaus, B. Ecker, D. Zimmer, V. Bagnoud, T. Kuehl, and C. Spielmann, "Laser-driven amplification of soft X-rays by parametric stimulated emission in neutral gases," Nat. Phys. **6**, 455-461 (2010).
6. J. Seres, E. Seres, and C. Spielmann, "Classical model of strong-field parametric amplification of soft x rays," Phys. Rev. A **86**, 013822 (2012).
7. J. Seres, E. Seres, B. Landgraf, B. Ecker, B. Aurand, A. Hoffmann, G. Winkler, S. Namba, T. Kuehl, and C. Spielmann, "Parametric amplification of attosecond pulse trains at 11 nm," Sci. Rep. **4**, 4254 (2014).
8. G. Gademann, F. Kelkensberg, W. Siu, P. Johnsson, K. J. Schafer, M. B. Gaarde, and M. J. J. Vrakking, "Attosecond control of electronion recollision in high harmonic generation," New J. Phys. **13**, 033002 (2011).
9. F. Brizuela, C. M. Heyl, P. Rudawski, D. Kroon, L. Rading, J. M. Dahlstrom, J. Mauritsson, P. Johnsson, C. L. Arnold, and A. L'Huillier, "Efficient high-order harmonic generation boosted by below-threshold harmonics," Sci. Rep. **3**, 1410 (2013).

1. Introduction

The simultaneous illumination of atoms with an intense infrared (IR) pulse and a weak extreme ultraviolet (XUV) pulse has been suggested as a means for table-top coherent XUV radiation sources with shaped attosecond pulses [1, 2] and with high photon energies via selective yield enhancement [3] in high-order harmonic generation (HHG) processes. The effect of XUV radiation combined with intense IR pulses on the HHG spectrum has been theoretically and experimentally investigated by several authors [5–9].

By using the strong field approximation (SFA) [4] it was shown in [3] that the HHG energy yield can be enhanced in a particular region of the spectrum when a weak XUV pulse is correctly phased and combined with the IR intense pulse producing high-harmonics. The theory predicted large enhancement for single 200 as pulses centered around 11 nm (113 eV). The enhancement effect is due to enhanced XUV nonlinear parametric forward scattering processes from the non-stationary electronic wave packet promoted by the intense IR driving field. Parametric amplification of attosecond pulse trains at 11 nm has recently been corroborated experimentally [7]. The measurements suggest that amplification takes place only if the seed pulse train is perfectly phased to the driving laser pulse in the amplifier, as predicted by the theory in [3].

In the present study we address the interaction of atoms with different ionization potentials, such as He, He^+ and Ne^{++}, with an intense infrared (IR) laser pulse combined with a weak extreme ultraviolet (XUV) pulse train. We investigate HHG processes together with nonlinear parametric amplification of the XUV pulse trains by performing a detailed study of the SFA theory in both the region around 100 eV and the *water-window* region around 300 eV. The later is specially relevant for x-ray spectroscopy techniques in medical and biological sciences. As it will be shown, we observe how although the HHG yield is largely affected by the particular ionization potential of the atom, stimulated processes from nonlinear parametric interactions are only weakly affected. Nonlinear parametric amplification is therefore easily observed in atoms of a high ionization potential such as He^+ and Ne^{++}. Furthermore, our simulations predict that XUV nonlinear parametric pulse amplification can be efficiently produced in the *water-window* spectral region, where the efficiency of HHG is poor.

2. Numerical simulations

The theoretical model that we consider is based on the single-atom response calculated by solving the Schrödinger equation in the strong field approximation (SFA) in the nonadiabatic form, so that the full electric field of the laser pulse is used to calculate the nonlinear dipole moment, which in the saddle-point approximation can be written as [4]

$$\begin{aligned} x(t) &= i\int_0^t dt' \left(\frac{\pi}{\varepsilon + i(t-t')/2}\right)^{3/2} \\ &\quad \times d_x^*[p_{st}(t,t') - A(t)] e^{-iS_{st}(t,t')} d_x[p_{st}(t,t') - A(t')] E(t') + c.c. \end{aligned} \tag{1}$$

The driving laser field in our study is composed of a strong femtosecond IR pulse $E_{IR}(t)$ and a weak attosecond XUV pulse train $E_{XUV}(t)$, so that $E(t) = E_{IR}(t) + E_{XUV}(t)$, and we have considered the dipole matrix element of hydrogenlike atoms for transitions to and from the continuum $\boldsymbol{d}(\boldsymbol{k}) = i(2^{7/2} I_p^{5/4}/\pi)(\boldsymbol{k}/(\boldsymbol{k}^2 + 2I_p)^3)$.

We specifically study the response of He (I_p = 24.59 eV), He^+ (I_p = 54.42 eV) and Ne^{++} (I_p = 63.45 eV) to an IR intense pulse combined with a weak XUV pulse. The IR field consists on a 10 fs laser pulse with a Gaussian temporal profile, carrier-envelope phase 0°, central wavelength of 800 nm, which produces high-order harmonics with a photon energy cutoff at $\approx 150 - 400$

eV depending on the atom and the IR peak intensity considered. The XUV field consists on a 10 fs envelope train of Gaussian 200 as pulses, delayed by half IR period, with carrier-envelope phase 0° and with a central wavelength well in the plateau of the generated HHG spectrum. We compute and compare the results in two different spectral regions: first we analyze the amplification of a XUV pulse train with central wavelength of 11 nm sent to the atomic gas target in combination with an IR pulse of 7×10^{14} W/cm^2 peak intensity, which results in a HHG cutoff at $\approx 150 - 200$ eV, depending on the atom considered. We then perform the simulations for a XUV pulse train with central wavelength of ≈ 4 nm and an IR pulse of 1.6×10^{15} W/cm^2, which results in a cutoff at $\approx 340 - 390$ eV, well in the *water-window* region (2.3 – 4.6 nm). Figure 1 shows the main results from the numerical simulations in the two different regions. In all the calculations the value of the XUV pulse peak intensity I_{XUV} is given by $I_{IR}/10^{12}$, with I_{IR} being the IR pulse peak intensity.

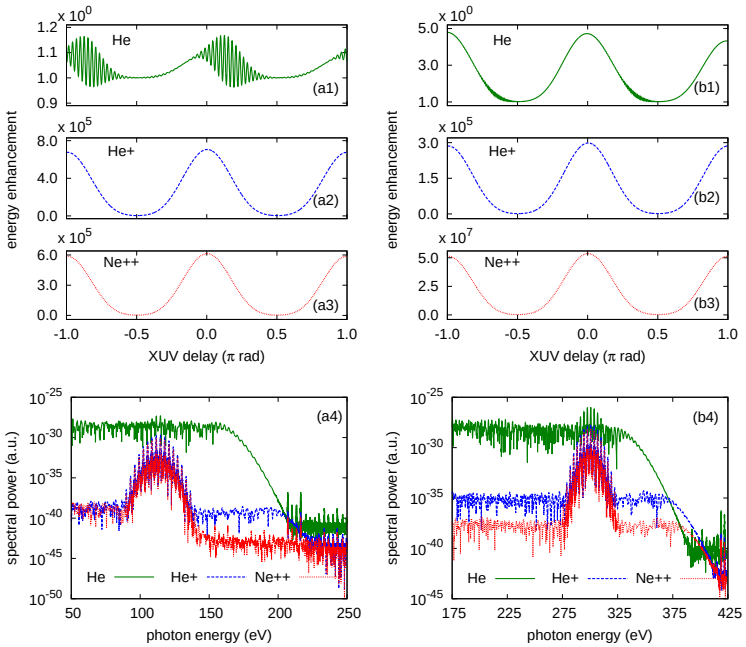

Fig. 1. (a1)–(a3) and (b1)–(b3): Energy enhancement of the HHG spectra caused by a 11 nm (a1)–(a3) and 4.13 nm (b1)–(b3) attosecond pulse trains for He (a1) and (b1), He^+ (a2) and (b2) and Ne^{++} (a3) and (b3), as a function of the delay between the IR and the XUV pulse train. (a4) and (b4): Spectra obtained by considering the combination of the IR 800 nm femtosecond strong pulse and the XUV weak pulse train for a 11 nm (a4) and a 4.13 nm (b4) pulse seed in the case of He, He^+ and Ne^{++}, as indicated.

Figures 1(a1)–1(a3) show the enhancement as a function of the time delay between the IR pulse and the XUV pulse train. The energy enhancement plotted in Figs. 1(a1)–1(a3) is defined as the ratio between the spectral energy obtained by using the combined IR+XUV pulses and the spectral energy obtained by using only the IR laser pulse, integrated in the region of the corresponding XUV spectral bandwidth. In the case of He^+ and Ne^{++} (Figs. 1(a2) and 1(a3), respectively) the behavior is similar to the one described in [3], which was observed for calculations assuming a single attosecond XUV pulse: the enhancement follows the shape of the IR electric field, so that there is a maximum enhancement at the delays that coincide with the

relative maxima (positive and negative) of the IR field carrier. In the case of He [Fig. 1(a1)] we observe fast oscillations that have a period coinciding with the XUV period, a behavior that was also reported in [3] for weak values on the XUV peak pulse intensity. This behavior is due to interference between the HHG signal and the amplified XUV signal, as it is clear if we look at the spectra shown in Fig. 1(a4). Indeed, in the case of He, as it is shown by the green full line in Fig. 1(a4) – and as it will be further commented below –, the yield from HHG is comparable to the amplified signal from the XUV pulse train, and hence oscillations from the interference of the two signals are present in the enhancement versus delay plot [Fig. 1(a1)]. In the case of He^+ and Ne^{++}, however, the HHG yield is very low compared to the amplified XUV signal, and therefore no fast oscillations are produced by interference [Figs. 1(a2) and 1(a3)].

It is worth noting that, as shown in Fig. 1(a4), the HHG yield is largely affected by the ionization potential of the atom. The HHG yield decreases by roughly 10 orders of magnitude in the case He^+ (54.42 eV) and Ne^{++} (63.45 eV) as compared to the case of He (24.59 eV). However, parametric XUV amplification is only weakly affected, decreasing by roughly 2 orders of magnitude [see Fig. 1(a4)]. This makes higher ionization potential atoms most optimal to observe the nonlinear parametric amplification phenomena, with enhancement factors as high as 10^5 for the parameter values used in the present simulations [see Figs. 1(a2) and 1(a3)].

The behavior that we observe for XUV amplification around 120 eV is robust when we increase the peak intensity of the IR laser pulse and the central photon energy of the XUV pulse train, as it is evident from the results shown in Figs. 1(b1)–1(b4). In Figs. 1(b1)–1(b3) we observe that the fast oscillations in the enhancement curve that were observed for He in the lower energy regime [Fig. 1(a1)] are not present. This is a consequence of the larger amplification that the XUV pulse train has experienced in this higher energy region and for the parameter values that are here used, as it can be seen in the corresponding spectrum [green full line in Fig. 1(b4)]. Therefore, we conclude that attosecond XUV amplification can be realized at the *water-window* spectral region and that it will be most optimally observed with atoms or molecules of a high ionization potential, such as those of He^+ and Ne^{++}.

3. Study of the different processes involved

In this section we will study the different processes that are involved in the interaction between the atom and the combination of the IR and the XUV pulses in the frame of the SFA. The time-dependent dipole moment in Eq. (1) can be written as $x(t) = x_{IR}(t) + x_{XUV}(t)$, with

$$\begin{aligned} x_{IR,XUV}(t) &= i\int_0^t dt' \left(\frac{\pi}{\varepsilon + i(t-t')/2}\right)^{3/2} \\ &\quad \times d_x^*[p_{st}(t,t') - A(t)] e^{-iS_{st}(t,t')} d_x[p_{st}(t,t') - A(t')] E_{IR,XUV}(t') + c.c. \end{aligned} \quad (2)$$

We have checked numerically that the response of the atom to the $E_{XUV}(t)$ field alone is very weak, so that the contribution from $x_{XUV}(t)$ to the total time-dependent dipole moment can be obviated when considering the combined $E_{IR}(t)$ and $E_{XUV}(t)$ fields. Therefore for the parameter values used in our study $x(t) \approx x_{IR}(t)$. In order to evaluate the different processes driving the time-dependent dipole moment, we can write the expression for $x_{IR}(t)$ as

$$\begin{aligned} x_{IR}(t) &= i\int_0^t dt' \left(\frac{2^{14}(2I_p)^5}{\pi(\varepsilon + i(t-t')/2)^3}\right)^{1/2} \\ &\quad \times \frac{d_1(t,t') + d_2(t,t') + d_3(t,t') + d_4(t,t')}{([p_{st}(t,t') - A(t)]^2 + 2I_p)^3([p_{st}(t,t') - A(t')]^2 + 2I_p)^3} e^{-iS_{st}(t,t')} E_{IR}(t') \\ &\quad + c.c., \end{aligned} \quad (3)$$

where $d_1(t,t') = [p_{st}(t,t') - A_{IR}(t)][p_{st}(t,t') - A_{IR}(t')]$, $d_2(t,t') = -[p_{st}(t,t') - A_{IR}(t)]A_{XUV}(t')$, $d_3(t,t') = -A_{XUV}(t)[p_{st}(t,t') - A_{IR}(t')]$ and $d_4(t,t') = A_{XUV}(t)A_{XUV}(t')$.

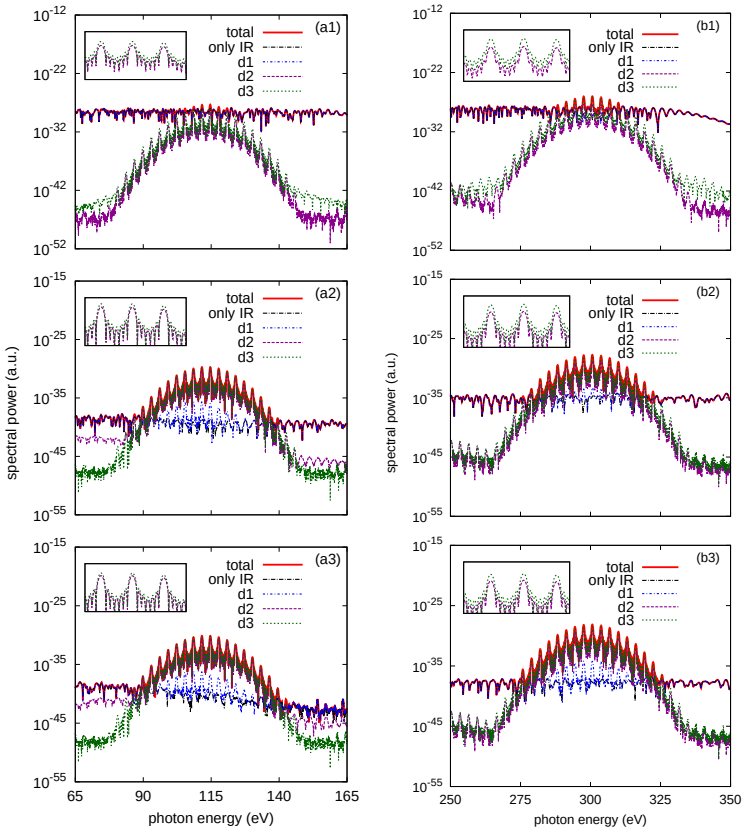

Fig. 2. Spectra obtained by considering the combination of the IR 800 nm femtosecond strong pulse and the XUV weak pulse train for a 11 nm (a1)–(a3) and a 4.13 nm (b1)–(b3) pulse seed (red thick lines), and spectra obtained by the Fourier transform of the acceleration of the time-dependent dipole moment in Eq. (3) considering the different contributions to the dipole matrix element $d_x(t,t')$, as indicated, in the case of He (a1) and (b1), He^+ (a2) and (b2) and Ne^{++} (a3) and (b3). The insets show the contribution of $d_2(t,t')$ and $d_3(t,t')$ at the central region of the plots around 115 eV (a1)–(a3) and 300 eV (b1)–(b3).

The decomposition of the dipole matrix element $d_x(t,t')$ in different factors gives us four integrals that can be computed separately. Readily, $d_1(t,t')$ accounts for the regular HHG processes, i.e. the spectrum that would be obtained in the absence of the E_{XUV} field. The processes described by $d_2(t,t')$ can be understood as nonlinear enhanced ionization due to the presence of the $E_{XUV}(t')$ pulse at time t', followed by propagation in the continuum from t' to t by the semiclassical action $S_{st}(t,t')$ and recombination at time t. The nonlinear parametric amplification process is produced by $d_3(t,t')$, which can be read as the probability for an electron to be ionized by the field $E_{IR}(t')$ at time t', propagated from t' to t by the semiclassical action $S_{st}(t,t')$, and recombined back to the ground state due to the presence of the attosecond pulse $E_{XUV}(t)$ at time t. The contribution from $d_4(t,t')$ is negligible. From Eq. (3) it is evident that the strength of the time-dependent dipole moment $x_{IR}(t)$ is proportional to the $E_{IR}(t)$ field strength, and both the $d_2(t,t')$ and $d_3(t,t')$ factors are proportional to the vector potential of the XUV field A_{XUV}.

As a consequence, the probability for $E_{XUV}(t)$ stimulated processes increases proportionally, on the one hand, to the $E_{XUV}(t)$ field strength, and on the other hand to the value of the $E_{IR}(t)$ field, which provides the energy for enhanced forward scattering of the $E_{XUV}(t)$ pulses.

Figure 2(a1) shows the spectrum calculated using the different contributions to the dipole matrix element, as given by the expressions for $d_1(t,t')$, $d_2(t,t')$ and $d_3(t,t')$. We have here considered the spectra resulting from the combination of the strong IR pulse ($I_{IR} = 7 \times 10^{14}$ W/cm^2) and the 11 nm XUV weak pulse train ($I_{XUV} = 700$ W/cm^2) interacting with He. The red thick line corresponds to the *total* dipole, i.e. the dipole calculated by using Eq. (1). The contribution to the spectrum from the $d_1(t,t')$ factor in Eq. (3) is shown by the blue dotted line in Fig. 2(a1). It is clear that this contribution corresponds to the HHG signal, since it does not show any amplification due to the $E_{XUV}(t)$ pulse train. The contribution from the nonlinear parametric amplification is given by $d_3(t,t')$. For all the parameters that we have considered $d_3(t,t')$ dominates in front of $d_2(t,t')$ – see the inset in Fig. 2(a1). Figures 2(a2) and 2(a3) show the same calculations for the case of He^+ and Ne^{++}, respectively. Clearly, the higher ionization potential of He^+ and Ne^{++} favors the observation of the nonlinear parametric amplification processes, since the contribution given by $d_2(t,t')$ and $d_3(t,t')$ is only weakly affected by the value of the ionization potential, while HHG is strongly reduced. In the case of He^+ and Ne^{++}, we observe a weak contribution in $d_1(t,t')$ from the $E_{XUV}(t)$ pulse train. This is shown by comparing the calculation performed with $d_1(t,t')$ with the one obtained by using only the IR pulse in the total integral in Eq. (3) [black full-dotted line in Figs. 2(a2) and 2(a3)]. This contribution, which is only visible for the lower HHG yield produced in He^+ and Ne^{++}, is due to the presence of the A_{XUV} factor in the stationary canonical momentum p_{st} in the denominator of the dipole matrix factors in Eq. (3). The physical meaning and relevance of this small contribution – which is negligible in the total calculation– is still under study.

In Figs. 2(b1)–2(b3) the study has been performed for the case of higher photon energies, i.e. by considering a higher value of the IR pulse peak intensity ($I_{IR} = 1.6 \times 10^{15}$ W/cm^2) and for a XUV pulse peak intensity such as $I_{XUV} = 1.6 \times 10^3$ W/cm^2, which in this case is centered at 300 eV. As it can be observed in Figs. 2(b1)–2(b3) the obtained spectra are hence well in the *water-window* region. The results that we observe in this high photon energy region are comparable to those obtained in the lower energy region – which have been described above–, and the dominance of $d_3(t,t')$ over $d_2(t,t')$ is even larger. Therefore we conclude that nonlinear parametric amplification is highly robust at high photon energies, and that higher ionization potentials such as those of He^+ and Ne^{++} will favor the observation of nonlinear parametric amplification processes.

4. Conclusions

We have performed a detailed study of strong-field mediated nonlinear parametric amplification of attosecond XUV pulses in the frame of the SFA. The results that we present around the 11 nm region were recently corroborated experimentally [7]. Our numerical simulations show that these nonlinear processes are robust at higher photon energies, such as in the *water-window* spectral region, and predict that x-ray amplification might be most optimally observed by using gas targets with high ionization potentials, such as He^+ and Ne^{++}, so that harmonics at a certain spectral range with high contrast can be generated compared to the broad spectrum of He.

Acknowledgments

Support from the Spanish Ministry of Economy and Competitiveness through "Plan Nacional" (FIS2011-30465-C02-02) is acknowledged.